Mars Helicopter Technology Demonstrator

J. (Bob) Balaram
Timothy Canham, Courtney Duncan, Matt Golombek, Havard Grip, Justin Maki, Amelia Quon, Ryan Stern, David Zhu
Jet Propulsion Laboratory, California Institute of Technology, 4800 Oak Grove Drive, Pasadena 91109, California, USA
Wayne Johnson, NASA Ames Research Center

We describe a helicopter that is being developed as a technology demonstrator of Mars aerial mobility. The key design features of the helicopter, associated test infrastructure, and results from a full-scale prototype are briefly described.

Nomenclature

ADC	Analog-to-Digital Converter
BIB	Battery Interface Board
COTS	Commerical Off-the-shelf
CPU	Central Processor Unit
dof	degrees-of-freedom
ECM	Electronics Core Module
EDM	Engineering Design Model
FC	Flight Controller
FFB	FPGA/Flight-Controller Board
FPGA	Field-Programmable Gate Array
GPIO	General Purpose Input/Ouput
GPS	Global Positioning System
IC	Integrated Circuit
IMU	Inertial Measurement Unit
MCU	Microcontroller Unit
MEMS	Microelectromechanical System
NAV	Navigation
NSB	Navigation/Servo Controller Board
ROI	Region of Interest
RTE	Return-to-Earth
SEL	Single-Event Latch-up
SOM	System On a Module
SPI	Serial Peripheral Interface
TCB	Telecommunications Board
UART	Universal Asynchronous Receiver/Transmitter

Units

C	degree Celsius
deg	degrees (angle)
ft	feet
g	gram
GB	Giga-byte
GHz	Giga-hertz
kg	kilogram
km	kilometer
K	Kilo
m	meter
mTorr	milli Torr
rpm	revolutions per minute
s, sec	second

sol	Martian day
Wh	Watt hour

I. Introduction

Aerial exploration of Mars with helicopters could provide mission capabilities that go beyond that of orbiting satellites, landed spacecraft and rovers. Helicopters allow examination of Mars at visual resolutions comparable to landers and rovers but over much longer ranges. They could access and land at designated targets in a controlled manner and could be used to carry or retrieve small payloads. Helicopters could enhance rover missions by quickly scouting out safe traverse routes or providing reconnaissance on possible science target destinations and, as standalone systems, could be used to explore areas that may not be reachable by rovers. Mars helicopters may also be considered as elements of a sample return architecture where they could be used for timely retrieval of small science samples back to a Mars ascent vehicle for return to Earth.

The challenge to helicopter use on Mars is the thin carbon dioxide atmosphere with approximately 1% of the density of Earth's atmosphere. Much like the Sojourner rover on the Pathfinder mission paved the way for the Spirit, Opportunity, Curiosity and the Mars 2020 rovers, an initial demonstration on Mars is desirable so as to inform the development of future helicopter missions. The Jet Propulsion Laboratory is leading a collaborative effort with AeroVironment Inc., and NASA centers Ames, Langley and Glenn to develop a small helicopter as a technology demonstrator. In this paper we briefly describe the results of this effort including results from controlled free-flight of a full-scale (approx 850 g) prototype flown in a test chamber under Mars conditions, the design and development of the 1800 g (not-to-exceed mass) technology demonstrator helicopter, and the operation of the helicopter.

II. Helicopter Models and Test Facilities

In May of 2016, a full-scale prototype (shown in Fig. 1) with a rotor diameter of 1.21 m was flown under simulated Mars atmosphere conditions in the JPL 25-foot diameter environment chamber. The helicopter was of a co-axial rotor design with a cyclic and collective on the lower rotor, and only a collective on the upper rotor. The test was conducted with the chamber evacuated to vacuum and backfilled with carbon-dioxide gas to a density of 0.0165 kg/m^3 (a representative density of the conditions that would be seen by the Mars vehicle). Because Earth's gravity at 9.81 m/s^2 is greater than Mars gravity at 3.71 m/s^2, it was not feasible to build the prototype to be the same mass as the Mars vehicle. Instead, items such as the power source and avionics were connected from the ground to the 850 gm vehicle through a light-weight electrical tether that was carried by the vehicle as it lifted off the ground. Sustained, autonomous, stable flight was achieved with the trajectory of the test flight shown in Fig. 2.

A. Experimental Campaigns

The JPL 25-ft Space Simulator chamber was used to test the helicopter prototype that was successfully flown in 2016. It is also in use to test the Engineering Development Model (EDM) of the Mars technology demonstrator design. The determination of thrust and power as a function of helicopter actuator settings, identification of key system dynamics, and controlled free-flight are the focus of the experimental campaigns.

Normally this facility is used to test spacecraft in a cold vacuum environment, but for helicopter flight dynamics testing this chamber is operated under Mars atmosphere conditions at ambient Earth temperatures. Actual Mars atmosphere conditions are significantly colder (e.g. approx -50 C), resulting in different blade aerodynamics conditions such as the Mach number. However, since the helicopter is operated with conservative tip Mach speeds (≤ 0.6), flight dynamics and performance results at ambient temperatures (e.g. approx 20 C) can be easily matched to the Mars conditions. The key parameter controlled in the chamber is the density of the CO2 atmosphere. The density value is selected to be in the expected operating range of the Mars vehicle and is achieved by pumping down the chamber to 500 mTorr before being backfilled with CO2 to a (approx 7 Torr) pressure that would match the required density.

The 25-ft diameter by 85-ft high Space Simulator is JPL's largest thermal-vacuum chamber. Even so, concerns about recirculation of rotor wash i.e. edge effects, led to a decision to characterize the helicopter's performance in an upside-down orientation to minimize recirculation effects. The helicopter was mounted 3.5 m above the floor on a test stand in a configuration that could simulate both hover flight as well as a forward flight. The helicopter was mounted on a carbon fiber arm that was held stationary to simulate hovering and swung in horizontal arcs to simulate the relative air-speed motion of forward flight. Initial system characterization tests were performed with the helicopter fixed to the

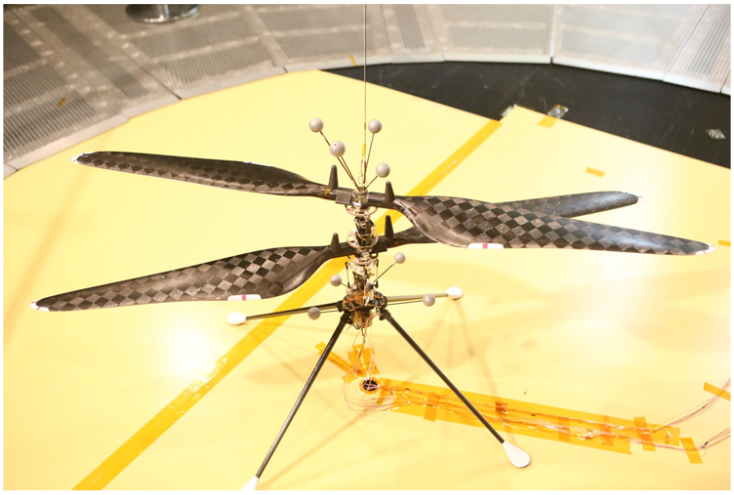

Fig. 1 Full-scale prototype of Mars Helicopter shown with safety tether (removed for free-flight tests), Vicon tracking targets, and electrical lines to off-board power and avionics.

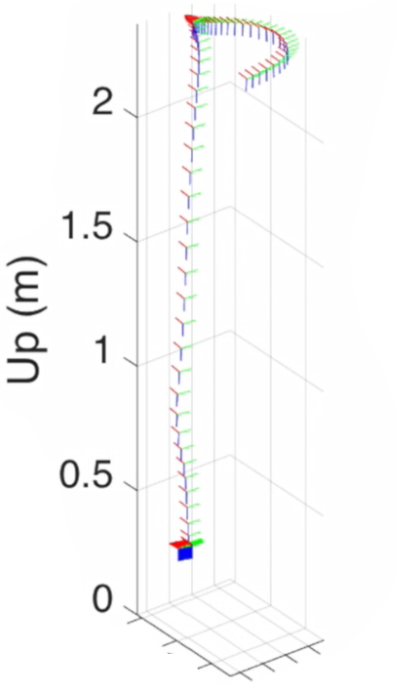

Fig. 2 Achieved flight profile of the Mars helicopter prototype. After ascent, the vehicle keeps station at a stable hover with some lateral motion that is the result of buffeting from the downwash flow in the limited confines of the test chamber.

end of the arm. Additional tests were conducted with the helicopter mounted on a custom 2-DOF gimbal at the end of the arm for additional system characterization and initial closed-loop attitude control testing. The test stand is shown in Fig. 3.

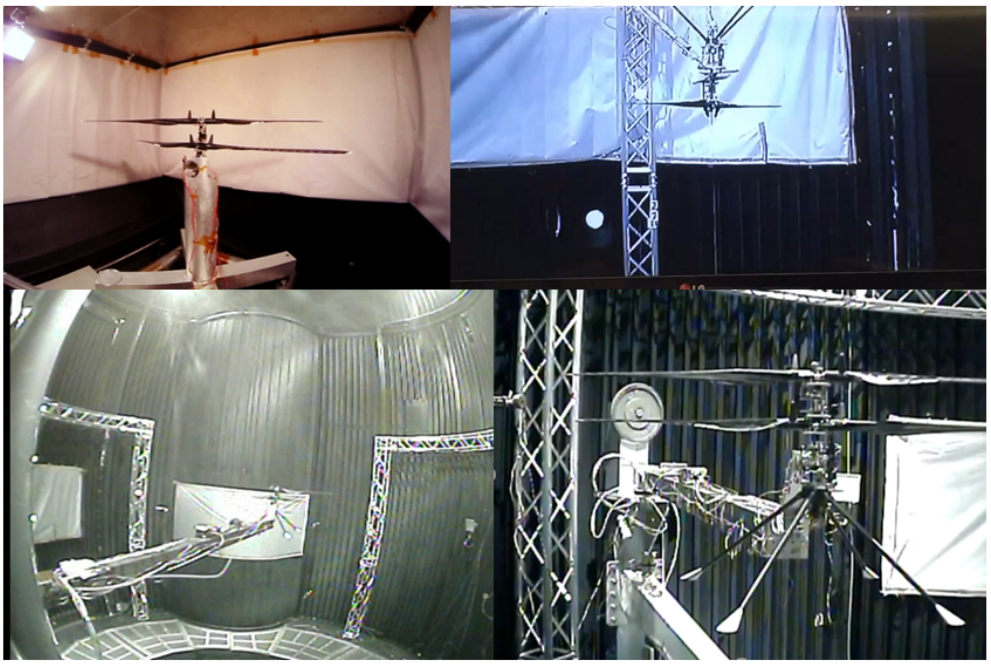

Fig. 3 Tests stand views (clockwise from upper left) include blade balancing, thrust measurement, translational dynamics swing-arm (closeup), and swing-arm operation

Associated metrology in the form of a force/torque sensor, a Vicon motion tracking system, stroboscopic lighting, a thermal camera, and temperature sensor monitors were developed to support operation in the chamber. The helicopter and test stand were instrumented with monitoring accelerometers and thermocouples. An infrared camera provided another means for monitoring the helicopter's performance. Pressing an emergency stop button in response to an over-threshold reading cuts power from the helicopter's power supplies to prevent damage.

The first full-scale prototype consisted of two rotors, one rotor motor and associated reversing gear train, and swash plate servos to control blade pitch. The control electronics were housed in Linux-based ground control computers, necessitating the use of an electrical umbilical cable connected to the helicopter at all times. The umbilical provided both power and commands to the helicopter system. In addition to an IMU (inertial measurement unit) sensor for attitude knowledge, the prototype also relied on a visual tracking system consisting of 18 Vicon cameras. These motion-tracking cameras use reflective sphere targets for motion capture. Eight of the reflective targets were mounted to the helicopter in a non-symmetric pattern. A separate ground computer monitored the attitude and location of the helicopter via the Vicon cameras and fed the data into the ground control computers.

The mass of this first prototype was approximately 0.75 kg allowing free-flight under Earth gravity conditions. For the Mars Technology demonstrator EDM at approximately 1.7 kg, free-flight is not possible without the lower gravity of Mars partially compensating for its thinner atmosphere by requiring less lift to fly a vehicle than would be required on Earth. To test fly a vehicle on Earth that was designed for Mars, a gravity offload system must be used to effectively reduce the weight lifted by the rotors. The offload system consists of a constant force motor (implemented by closed-loop sensing of line tension) and a reel fitted with Dyneema filament.

III. Flight Control Challenges

Designing a robust control system for a helicopter is a challenging task in general, due to various unusual characteristics of helicopters as compared to other vehicles. In particular, helicopters are typically unstable in open loop, exhibit significant coupling between different vehicle axes, and are subject to high levels of vibration. The control design problem becomes more challenging when, as in the case of the Mars Helicopter, the vehicle must take off and land on unprepared terrain and navigate without external aids such as GPS. Most challenging of all, however, are those aspects that are unique to flying on Mars:

- The atmosphere and gravity are dramatically different from Earth.
- Little prior information exists on how these differences affect the flight dynamics in the Martian environment.
- The environment cannot be fully replicated for testing on Earth.
- The helicopter control system must work the very first time it operates in its intended environment.

As a result of the above, we are forced to rely on detailed modeling, analysis, and simulation, combined with testing in partially replicated environments. Simple analytical models and scaling arguments are helpful in understanding the fundamental differences between Earth and Mars helicopter flight. This analysis is extended with high-fidelity modeling combining multi-body dynamics with aerodynamic modeling, which guides both the design of the vehicle and the control algorithms. Finally, *system identification* experiments are carried out in various test configurations inside a vacuum chamber at Mars density, in order to determine key properties of the actual helicopter dynamics.

A. Mars Helicopter Flight Dynamics

The key parameter affecting the aerodynamic properties of the Mars Helicopter is the density, which is 1-2% of Earth density at sea level. Clearly, the thin atmosphere reduces the achievable thrust for a given rotor size; beyond that, however, it also affects the flight dynamics of the vehicle in ways that must be well-understood in order to design a control system.

Besides gravity, the main forces on a helicopter are due to the rotor interacting with the surrounding atmosphere. The rotor is a dynamical system whose properties largely determine the flight characteristics of the vehicle as a whole. Of particular importance for the helicopter flight dynamics is the dynamics of rotor blade *flapping*; that is, the out-of-plane motion of the rotor blade that occurs when the blade is subjected to forces. Many helicopters have hinges that allow the blade to flap, but even for hingeless helicopters like the Mars Helicopter, blade flapping occurs due to elastic deformation of the blade.

The thin Martian atmosphere significantly affects the dynamics of blade flapping by reducing the level of aerodynamic damping. This alters the response of the helicopter rotor to periodic inputs, including cyclic control inputs; in particular, the forces and moments on the helicopter fuselage in response to such inputs tend to be oriented differently when compared to similar inputs on Earth helicopters. Furthermore, the poorly damped flap dynamics gives rise to poorly damped, oscillatory modes in the overall flight dynamics, called the *regressing* and *advancing* flap modes. The existence of such modes represents a problem due to the danger of the control system coupling with the modes and potentially destabilizing them. Due to this issue, it was determined early in the design process that the Mars Helicopter would need to be designed with unusually stiff blades, with a rotating flap frequency of about 80–90 Hz. This has the effect of moving the poorly damped modes to frequencies high enough not to interfere with the control system.

A drawback of the stiff rotor design is an increased sensitivity to gusts, which also worsens the open-loop unstable behavior of the helicopter. For more in-depth information about Mars Helicopter flight dynamics, see [1].

B. Modeling and Simulation

To capture the helicopter dynamics with high levels of fidelity, nonlinear modeling and simulation tools are needed.

1. HeliCAT

The primary tool for studying flight dynamics for the Mars Helicopter is called *Helicopter Control Analysis Tool* (*HeliCAT*). It was developed specifically for this purpose, using the *Darts/Dshell* multibody simulation framework developed at JPL (see, e.g., [2]). The strength of HeliCAT is in the features tailored toward GNC design, including detailed modeling of actuators and sensors, ground contact dynamics, ground support equipment, flight software integration and 3D visualization. The simulations were used to generate and verify key mechanical design requirements such as rotor stiffness, perform system identification of vehicle dynamics to develop control algorithms, test embedded flight-software, and rehearse all test efforts. Parameters obtained from system identification were used to design the

controller and excellent agreement between simulation and free-flight data was obtained. Fig. 4 shows a snapshot of simulated Mars flight within Victoria crater on Mars.

Fig. 4 HeliCAT visualization of the helicopter flying on Mars, with flight software in the loop.

2. CAMRAD II

Validation and additional high-fidelity studies are performed using CAMRAD II, a comprehensive analysis tool for rotorcraft that is widely used across NASA and in industry [3–5]. The CAMRAD II aerodynamic model for the rotor blade is based on lifting-line theory, using steady two-dimensional airfoil characteristics and a vortex wake model, plus models for unsteady flow (attached flow and dynamic stall) and yawed/swept flow. Effects of compressibility (Mach numbers) and viscosity (Reynolds number, stall and drag) enter through airfoil table data: lift, drag, moment coefficients of two-dimensional sections as function of angle of attack and Mach number, for the appropriate chord and atmosphere (density, temperature) so as to have correct Reynolds number variation with Mach number. The vortex wake consists of rolled-up tip vortices and inboard vortex sheets, emanating from each blade. Second-order lifting-line theory gives the vortex-induced loading on the blades well. Free wake geometry calculations give the self-induced distortion of the inter-twined, interacting tip vortices, including the mutual interaction of the wake from the two coaxial rotors. Accurate modeling of the distorted wake geometry is required for calculation of rotor performance, as well as structural loads and vibration. The interaction of coaxial rotors improves hover performance by 5-8% relative a single rotor with the same blade number and area. The CAMRAD II blade structural model is based on nonlinear beam theory of rotating finite elements. Modal characteristics of the blade can be calculated in vacuum and with aerodynamic forces. The trim task finds the equilibrium solution for a steady state operating condition (periodic blade loading and motion), and produces the solution for performance, loads, and vibration. The flutter task linearizes the equations about the trim solution, and produces stability results. CAMRAD II has undergone extensive correlation of performance and loads measurements on rotorcraft, including coaxial rotors [6].

Performance: The rotor was designed using an analysis for the optimum induced power of a propeller, at low axial speed to simulate hover operation, and with the two-bladed coaxial rotor modeled as a single four-bladed rotor. CAMRAD II performance calculations were used to assess the influence of the discrete tip vortices in hover, and the interactions between the two rotors in coaxial configuration. These calculations influenced the twist of the final design. Subsequent calculations identified high drag at the tip due to tapering outboard of 95% radius; showed the benefits of changing the taper, trading less inboard chord for more outboard chord to get larger thrust-weighted solidity at the same weight; and considered the impact of using airfoil shapes more appropriate for these low Reynolds numbers (the optimum section shape at Re<10000 often is a cambered flat plate). Further optimization of the blade planform, twist, and airfoil shape would have improved the rotor figure of merit, perhaps by 5%. The chamber test of May 2016 demonstrated that the performance of the rotor system will be adequate to achieve the goals of the technology demonstration, so the rotor aerodynamic and structural design was frozen and resources directed to other aspects of aircraft development. In

support of the testing, CAMRAD II performance results were used to identify the rotor operating point in terms of power and thrust with allowance for control.

Blade structural dynamics: HeliCat models the blade as a rigid structure with a flap hinge. CAMRAD II was used to calculate the mode shapes and frequencies of the rotating elastic blade. Comparing with results for a rigid blade, the flap hinge radial station and orientation and spring were identified for use in the HeliCat rotor model. It was also observed that inboard part of the blade is very stiff, most of the blade deflection occurring outboard of 50% radius, indicating that it should be possible to reduce the blade weight by tailoring the inboard stiffness.

Rotor dynamic response: CAMRAD II was used to calculate the rotor response to gust and control input, for comparison with the HeliCAT model. Several modeling features were adjusted as a result, including incorporation of section unsteady aerodynamics, yawed flow, and tip losses in the blade aerodynamic model. The impact of dynamic inflow models was also examined, with the final HeliCat calibration based on identification from the test data.

3. Computational Fluid Dynamics Analyses

High-fidelity aerodynamic calculations were performed to support the design and testing. In the absence of test data for airfoils at low Reynolds number and high Mach number, airfoil tables for the rotor (including thick inboard sections) were generated using CFD. Calculations were performed using the codes FLUENT, OVERFLOW, and ARC2D/C81GEN. There was generally good agreement between the results of these methods, although differences were found post stall [7]. To support the development of the HeliCat model, performance and hub loads were obtained from calculations using OVERFLOW. Interactions between rotor and the test chamber were calculated using the mid-fidelity analysis RotCFD [8]. These results were used to identify the optimum configuration for performance testing.

C. System Identification

Despite the best efforts to understand the Mars Helicopter flight dynamics using modeling and simulation tools, the results cannot be considered reliable enough to be the sole basis for control design. Therefore, a *system identification* campaign is conducted in Mars atmospheric conditions to determine the dynamics of the actual vehicle. System identification for the Mars Helicopter demonstration vehicle was performed in three main configurations: locked down on a force-torque sensor, where the controls were exercised and the reaction forces and moments were measured; on a swinging arm, where the forces and torques in response to airflow over the rotor were measured; and on a gimbal, where actual vehicle motion in response to control inputs was measured. This process revealed several important properties, including larger-than-expected sensitivity to edgewise flow over the rotor, and negative (i.e., unstable) damping factors in roll and pitch. Additional information on modeling, simulation, and system identification for the Mars Helicopter can be found in [1].

D. Guidance, Navigation, and Control Architecture

Fig. 5 illustrates the high-level architecture of the guidance, navigation, and control subsystem. Based on commands from a ground station, the *Mode Commander* is responsible for setting the mode of the other software modules according to the current the phase of flight, as well as initiating any actions associated with transitions between modes (e.g., planning of a new trajectory). The *Navigation* module uses sensor data to estimate the state of the vehicle, which is used by the *Control* module, and intermittently by the *Guidance* module and the Mode Commander. The Guidance module produces reference trajectories and feedforward control signals based on the current phase of flight. The control module adds feedback control based on the difference between the reference trajectories and the estimated state, which yields the actuator commands.

The Mode Commander is designed as a finite state machine, with states that align largely with the phases of flight (e.g., takoff, climb, hover). The guidance module generates consistent vehicle trajectories with limits on velocity, acceleration and jerk, which are converted into reference trajectories for individual states as well as control feedforward. The navigation system uses the onboard IMU for state propagation, and combines it with data from the downward-looking navigation camera and the altimeter to limit drift in position, velocity, and attitude. The control module is designed according to a nested architecture, with an outer translational control loop feeding reference signals to an inner attitude loop. For further details, see [9].

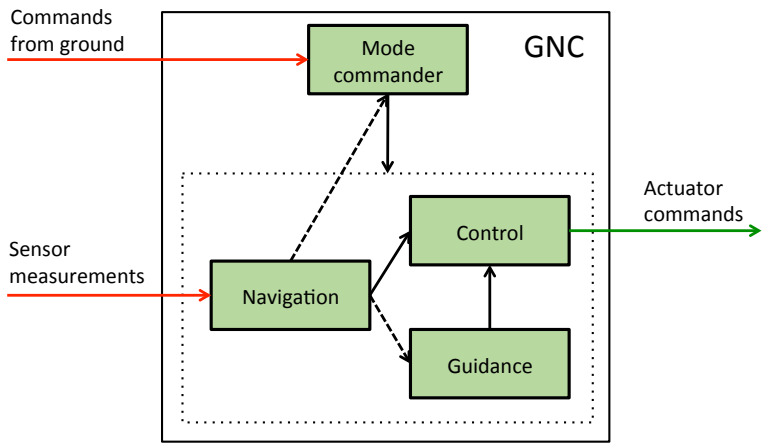

Fig. 5 High-level GNC architecture. Red arrows illustrate information flowing into the system; green arrows illustrate information flowing out of the system; solid black arrows illustrate continuous information flow within the GNC system; dashed black arrows illustrate intermittent information flow within the GNC system.

IV. Mars Helicopter Engineering Development Model

The size of the technology demonstrator vehicle at 1.21 m rotor diameter is selected to minimize accommodation and deployment related constraints imposed on any host spacecraft which would carry the helicopter to Mars. The accommodation on the host spacecraft and deployment from the stowed location of the helicopter are important drivers for the helicopter design. A reliable system incorporating electromechanical and/or pyrotechnic elements is needed to reposition and orient the helicopter from its stowed location, release any restraints for blades or legs, and drop the helicopter onto the ground. In this paper we do not discuss the details related to accommodation and deployment as these are specific to the host spacecraft. It is expected, however, that once deployed as a standalone system on the Mars surface, the demonstration vehicle would use a base station communications relay mounted on the host spacecraft to communicate to and from Earth.

All components of the helicopter must satisfy *Contamination Control* requirements i.e. they need to be selected to prevent out-gassing in the vacuum of space producing products that could contaminate other spacecraft elements. In addition all elements must also meet *Planetary Protection* requirements i.e. they need to incorporate treatments and handling procedure to prevent bio-contamination of instruments and sites with Earth organisms.

The EDM of the technology demonstration vehicle incorporates all the features of the final design (Fig. 6) and its features are now discussed in more detail.

A. Rotor System

The rotor system provides lift for the helicopter as well as forces required for the directional control of its trajectory. The design uses a 1.21 m diameter coaxial counter-rotating rotors with a rigid rotor i.e. no flap or lag hinges. The rotor is very stiff with a very high flap frequency (better than 1.9/rev) so as to mitigate some of the control challenges identified earlier. There are swashplates on both the upper and lower rotor, each with collective and cyclic control. The collective angle can range from -4.5 deg to 17.5 deg and the cyclic angle has a range of $\pm 10\ deg$. The maximum rotation rate for the rotors is 2800 rpm.

The rotor is shown in Fig. 7 and is fabricated from carbon fiber composites for most of the primary structure. The blades use a low Reynolds number airfoil with optimized twist and chord. Seals around bearings and a soft boot around the swashplate assembly mitigate against dust in the Mars atmosphere. Actuator power electronics are co-located with each actuator, and the motors self-heat before flight. The rotors are actuated with a custom 46 pole brushless motor with solenoid wound teeth using rectangular copper wire. Three Maxon brushed DC motors (DCX10) operating through a 4-stage gear-box control the height and tilt of each swashplate. Chinese weights provide a restoring force on the blade moments when under centrifugal loads thereby reducing the torque requirements on the swashplate actuators.

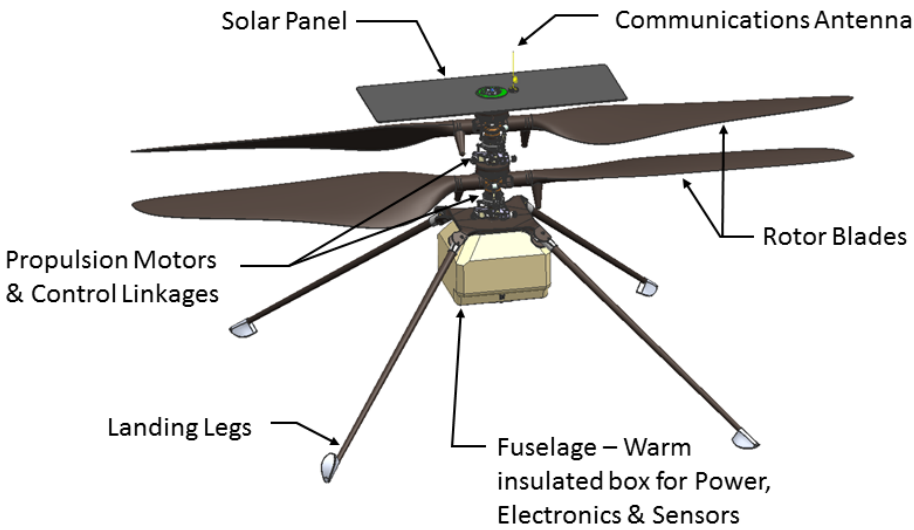

Fig. 6 Engineering Demonstration Model Design

B. Structure

The helicopter is built around a central mast - a hollow structural tube that runs from the top of the helicopter to the bottom. Within this tube are the wires from the Electronics Core Module (ECM) to the propulsion motor and servo elements, as well as to the host spacecraft. The mast tube is designed to be stiff so as to minimize control interactions, as well as have low thermal conductivity to minimize thermal leakage into the ECM.

Attached to the mast are (ordered from top to bottom):

- Upper Launch Lock. This attaches the helicopter to the host spacecraft prior to deployment onto the surface. Attached to the launch lock are deployment devices, wires to provide power and communications prior to deployment, and separation connectors to cleanly disconnect electrical lines upon deployment.
- Solar Panel. The solar panel substrate is attached to the mast and the cells are mounted onto this substrate.
- Upper & Lower Rotors. The rotor hubs are attached to the mast and includes the various non-rotating elements such as the servos, the non-rotating portion of the swashplate, the rotor windings, and the rotor power electronics.
- Landing Gear Mounting Plate. This consists of a plate to which are connected 4 light-weight legs.
- Fuselage Warm Electronics Box. The fuselage consists of a very lightweight structural frame to hold the thermal skin of the helicopter, and the 30 mm gap insulation between the skin and the ECM.
- ECM Assembly. The ECM (Figure 8) is mounted onto the mast and consists of the battery, the Battery Interface Board (BIB), and electronics circuits board for the avionics.
- Upper Sensor Assembly. This consists of an inclinometer, IMU and associated vibration isolation elements mounted on the mast as close to the center-of-mass of the vehicle (to minimize the effects of angular rates and accelerations). The Lower Sensor Assembly (consisting of an altimeter, cameras and a secondary IMU) is mounted directly onto the ECM and not onto the mast.
- Lower Launch Lock. This holds the helicopter to the host spacecraft on the other end prior to deployment.

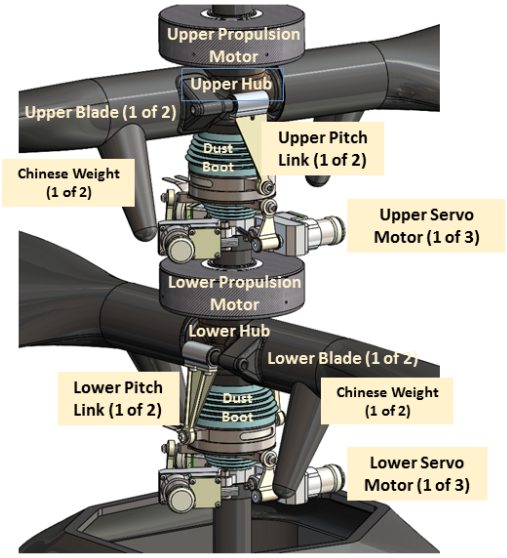

Fig. 7 Rotor assembly

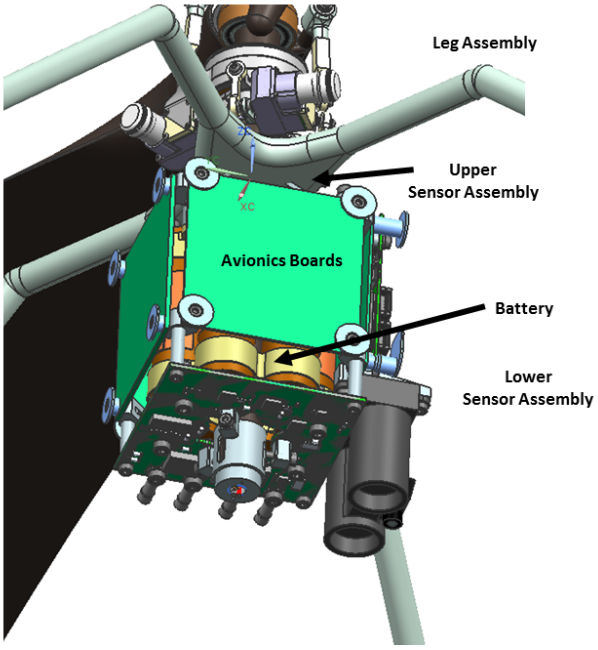

Fig. 8 Electronics Core Module (ECM) showing configuration of battery surrounded by avionics boards and attached sensor assemblies. Note that the upper sensor assembly is not visible in this view

C. Avionics Computing

A three-level fault-tolerant computing architecture is used on the helicopter as shown in Fig. 9. Software is implemented using the Instrument Software Framework [10].

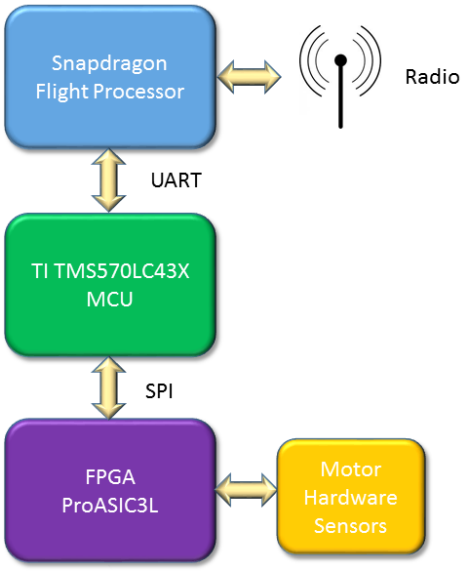

Fig. 9 Block Diagram of Avionics Elements

1. Processors

The Snapdragon™ processor from Intrinsyc® with a Linux operating system performs high-level functions on the helicopter. The Snapdragon™ processor has a 2.26 GHz Quad-core Snapdragon™ 801 processor with 2 GB Random Access Memory (RAM), 32 GB Flash memory, a Universal Asynchronous Receiver Transmitter (UART), a Serial Peripheral Interface (SPI), General Purpose Input/Ouput (GPIO), a 4000 pixel color camera, and a Video Graphics Array (VGA) black-and-white camera. This processor implements visual navigation via a velocity estimate derived from features tracked in the VGA camera, filter propagation for use in flight control, data management, command processing, telemetry generation, and radio communication.

The Snapdragon™ processor is connected to two flight-control (FC) Microcontroller Units (MCU) via a Universal Asynchronous Receiver/Transmitter (UART). These MCU processor units operate redundantly, receiving and processing identical sensor data to perform the flight-control functions necessary to keep the vehicle flying in the air. At any given time, one of the MCU is active with the other waiting to be hot-swapped in case of a fault. The MCU from Texas Instruments is a TMS570LC43x high-reliability automotive processor operating at 300 MHz, with 512 K RAM, 4 MB flash memory, UART, SPI, GPIO.

2. Avionics Boards

The avionics consists of 5 printed circuit boards which form the 5 facets of the ECM (Electronic Core Module) cube, enclosing the 6-cell lithium-ion battery pack. The boards are shown in Fig. 10.

The bottom of the cube is the battery interface board (BIB), which is attached to the battery and hosts the battery monitoring circuitry, motor power switches and motor current monitors. The battery and the BIB can be detached from helicopter and is intended to be replaceable.

The remaining 4 boards are the FPGA/Flight Controller Board (FFB), the NAV/Servo Controller Board (NSB), the Telecom Board (TCB) and the Helicopter Power Board (HPB):

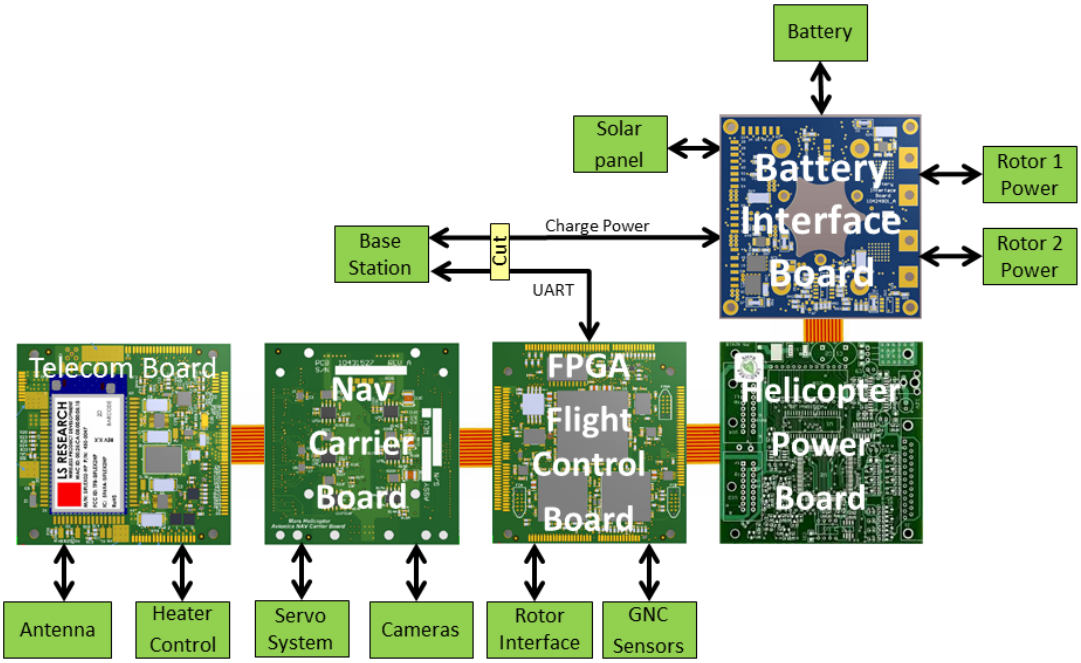

Fig. 10 Avionics Boards shown in unfolded configuration together with key interfaces

- **FFB**. The FFB is at the heart of the ECM. The two redundant TI Hercules safety processors serve as the low-level flight controller (FC); each has dual-core lockstep ARM Cortex-R5F and ECC protected Flash and RAM. The two processors run in sync and are provided with the same clock and data by the FPGA, which handles all the sensors and actuators interface. The lockstep mechanism does cycle by cycle error detection. If a fault is detected, it signals the error to the FPGA; the FPGA switches to the other processor and power cycles the faulty one, so the flight control software continues to run without disruption. The analog signals are digitized by the two independent 12-bit ADCs in each of the flight controllers.
- **NSB**. The NSB carries the Snapdragon CPU as a System on a Module (SOM) and provides power and I/O interfaces which include 3 UARTs, 1 SPI and a few discrete GPIOs. The NSB also hosts the drive circuitry for the 6 DC servo motors and delivers over 20 W power.
- **TCB**. The COTS telecom module is mounted on the TCB. Some additional analog circuitry, a 16-bit 8-channel ADC, the temperature sensor interface and heater switches take up the remaining space. This ADC is used for monitoring charging current and temperature without having to turn on the FCs, thereby saving power.
- **HPB**. The HPB has two DC/DC converters that regulate the battery voltage to the 3.3 V and the 5 V. The 5 V regulator can be switched off.

Although COTS electronics parts are used, selections are made for military-grade, automotive or industrial grade with the operating temperature range of at least -40 C to +85 C. The ICs are screened for single-event latch-up (SEL) and parts are also selected for low power. Each subsystem has a current monitor to detect possible latch-up current and can be power cycled to clear a SEL. In addition, current limiting is added to prevent a destructive SEL event and most devices are switched off when not in use to minimize their exposure to SEL. For the critical FPGA which is always on for the duration of the mission, the radiation tolerant ProASIC3 is chosen with the military temperature grade (-55 C to 125 C) and -1 speed grade to mitigate the degradation in the propagation delay caused by the total dose radiation. The single-event upset (SEU) is mitigated with triple module redundancy (TMR) in the FPGA design.

3. FPGA

At the heart of the helicopter avionics is a Field-Programmable Gate Array (FPGA). The FPGA implements the custom digital functions not implemented in software due to resource limitations of the processors (e.g. I/O or bandwidth limits), timing requirements, power considerations, or fault tolerance considerations. The FPGA device is a military-grade version of MicroSemi's ProASIC3L, which uses the same silicon as the radiation-tolerant device from the same family. The FPGA perform all critical I/O to the sensors and actuators, and fault managment functions including detecting error flags from the MCU and hot-swapping to functioning MCU in case of an error.

The FPGA performs vehicle flight control including an attitude control loop operating at 500 Hz, an outer motor control loop, waypoint guidance, sensor I/O from the IMU, altimeter and inclinometer, and analog telemetry for current and temperature sensing. It is responsible for system time management, interfaces to the IMU, altimeter and inclinometer sensors. It implements the "inner" motor control loop used for the two brushless rotor motors and the six brushed motor servos (three at each rotor swashplate), as well as power management and thermal control functions.

Most communication on the helicopter avionics flows through the FPGA. The FPGA implements 25 separate serial data interfaces (SPI, I2C, UART, SENT) to enable multiple paths of communication between the three processors, GNC devices (both IMUs, altimeter, inclinometer), all 8 motors, battery monitor, and external ADC. During cruise, and prior to deployment, the helicopter FPGA communicates to the FPGA on the base station to report telemetry.

Once the helicopter is deployed from the host spacecraft, the FPGA manages the power and operational state for the entire helicopter. It turns on and off the other avionics elements as they are needed, implements thermostat control of the survival and operational heaters, monitors the battery cell voltages, and performs cell balancing. Being one of only two elements that is always powered post-deployment (the other is the battery monitor), the FPGA maintains precision spacecraft time, implements alarm clock functions, and generates real-time interrupts for the rest of the system.

The helicopter FPGA implements most of the fault protection on the vehicle. It collects telemetry and health status from a variety of sources and responds to them as a function of the operational state. It operates the pair of FC processors as a primary and hot spare, determining when to switch from one to the other, and restoring critical state data to a processor after it has been power cycled. Critical data used by any of the processors is stored in the FPGA. Triple module redundancy is applied to critical flip-flops, as resources permit, to add additional protection from SEU.

Helicopter motor control is divided between the FPGA and software. For each of the six, brushed DC motor servo controllers, the FPGA generates the PWM drive signals and reads the absolute position sensor. For the two brushless DC rotor motors, the FPGA implements the commutation loop, driving the motors with space vector PWM (SVPWM). A closed-loop angle tracker produces a rate measurement and a smooth, low-lag, angle measurement from the Hall signals that feeds into the SVPWM algorithm. The FPGA also implements novel approaches to compensate for the inductive lag of the motor and calibrate out variations of the Hall sensors.

D. Sensors

On-board sensors are used for vehicle control during all phases of flight. Data from IMU's, an altimeter, and navigation camera image derived velocimetry is used to produce a navigation solution consisting of helicopter position, velocity, attitude, and other auxiliary variables. An inclinometer is used on the ground prior to flight to calibrate the IMU accelerometers biases. The helicopter also carries a color camera to provide images of terrain and other features for return to Earth.

The sensors used are Commercial-Off-The-Shelf (COTS) products:

- IMU. These are two 3-axis MEMS device from Bosch (Sensortec BMI-160), one for the upper sensor assembly in a vibration isolation mount, and one on the lower sensor assembly where it is co-located with the cameras.
- Inclinometer. This is a 2-axis MEMS MuRata device (SCA100T-D02)
- Altimeter. This is a time-of-flight altimeter with a range of 10's of meters from Garmin (Lidar-Lite-V3).
- Navigation (NAV) Camera. This is a global-shutter, nadir pointed grayscale 640 by 480 pixel sensor (Omnivision OV7251) mounted to a Sunny optics module. It has a field-of-view (FOV) of 133 deg (horizontal) by 100 deg (vertical) with an average Instantaneous Field-of-view (IFOV) of 3.6 mRad/pixel, and is capable of acquiring images at 10 frames/sec. Visual features are extracted from the images and tracked from frame to frame to provide a velocity estimate.
- Return-to-Earth (RTE) Camera. This is a rolling shutter, high-resolution 4208 by 3120 pixel sensor (Sony IMX 214) with a Bayer color filter array mated with an O-film optics module. This camera has a FOV of 47 deg (horizontal) by 47 deg (vertical) with an average IFOV of 0.26 mRad/pixel.

Both cameras are mounted on the helicopter Lower Sensor Assembly as shown below in Fig. 11. The NAV camera

is pointed directly towards nadir, and the RTE camera is pointed approximately 22 deg below the horizon, resulting in an overlap region between the two camera image footprints of approximately 30 deg × 47 deg. The overlap allows the possibility of feature registration between NAV and RTE images during post-flight data processing on Earth.

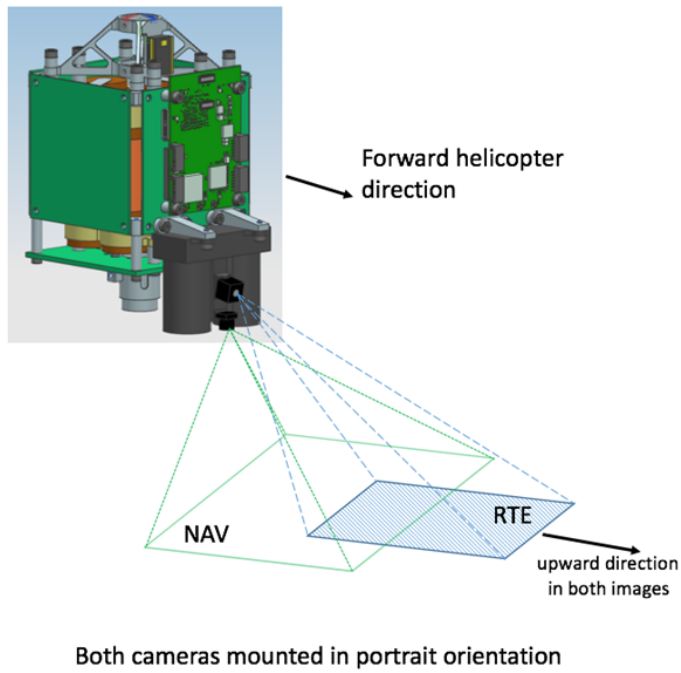

Fig. 11 Location and mounting of helicopter cameras.

The cameras were tested for thermal and radiation survivability as part of a test and selection effort from a larger group of candidate COTS hardware. Under typical Martian surface illumination levels the camera exposure times are expected to be on the order of a few milliseconds, depending on the time of day and details of the exact scene (e.g., surface albedo, shadows, etc.). The cameras are protected by dust and debris by a clear window (not shown in the figure). Images from the cameras are read directly into the navigation computer over a MIPI connection, and any image data sent back to Earth will undergo JPEG compression prior to being relayed to the host spacecraft.

E. Landing System

The landing system consists of 4 legs made of tapered carbon fiber/epoxy tubes. The feet are designed to prevent the leg from digging into soft landing surfaces. They also provide some damping by scrubbing against the ground as the leg flexes. Additional energy absorption is provided by flexible deforming elements at the hinges connecting the legs to the landing gear mounting plate which is affixed to the mast. The leg designs are tested against a variety of Martian surfaces ranging from hard rock to deep sand.

The landing system provides for a passive drop onto the ground from a height 0.3 m with only limited attitude rate control active during the final contact event with the ground. This minimizes ground-control interactions that could de-stabilize the helicopter. The landing gear is designed to allow the landing on surface with slopes upto 10 deg in any direction with the vehicle at an additional roll (or pitch) angle of 30 deg. Vertical velocity at the height where the passive gravity drop is initiated can be as high as 2.5 m/s with final vertical touchdown velocity as high as 3.5 m/s. A horizontal velocity of upto 0.5 m/s can be present due to delivery errors in the control system.

F. Telecommunication System

Once separated from the host spacecraft (lander or rover), the Mars Helicopter can only communicate to or be commanded from Earth via radio link. This link is implemented using a COTS 802.15.4 (Zig-Bee) standard 900 MHz chipset, SiFlex 02, originally manufactured by LS Research. Two identical SiFlex parts are used, one of which is an integral part of a base station mounted on the host spacecraft, the other being included in the helicopter electronics. These radios are mounted on identical, custom PC boards which provide mechanical support, power, heat distribution, and other necessary infrastructure. The boards on each side of the link are connected to their respective custom antennas. The helicopter antenna is a loaded quarter wave monopole positioned near the center of the solar panel (which also serves as ground plane) at the top of the entire helicopter assembly and is fed through a miniature coaxial cable routed through the mast to the electronics below. The radio is configured and exchanges data with the helicopter and base station system computers via UART.

One challenge in using off-the-shelf assemblies for electronics systems to be used on Mars is the low temperatures expected on the surface. At night, the antenna and cable assemblies will see temperatures as low as $-140\ C$. Electronics assemblies on both base station and helicopter will be kept "warm" (not below $-15\ C$) by heaters as required. Another challenge is antenna placement and accommodation on the larger host spacecraft. Each radio emits approximately 0.75 W power at 900 MHz with the board consuming up to 3 W supply power when transmitting and approximately 0.15 W while receiving. The link is designed to relay data at over-the-air rates of 20 kbps or 250 kbps over distances of up to 1000 m.

A one-way data transmission mode is used to recover data from the helicopter in real time during its brief sorties. When landed, a secure two-way mode is used. Due to protocol overhead and channel management, a maximum return throughput in flight of 200 kbps is expected while two-way throughputs as low as 10 kbps are supported if required by marginal, landed circumstances.

G. Power & Energy System

The helicopter is powered by a Li-Ion battery system that is recharged daily by a solar panel. The energy in the battery is used for operating heaters to survive the cold Martian nights as well as operate the helicopter actuators and avionics during short flights lasting from 90 seconds to a few minutes. Depending on the latitude of operations and the Martian season, recharging of this battery through the solar panel could occur over one to multiple sols (Martian days).

The helicopter battery shown in Fig. 12 consists of 6 Sony SE US1865o VTC4 Li-ion cells with a nameplate capacity of 2 Ah. The maximum discharge rate is greater than 25 A amd the maximum cell voltage specified by the manufacturer is 4.25 V. The continuous tested power load capability of this batterry is 480 W with a peak power capability of 510 W. Battery voltage is in the range of 15–25.2 V and the total mass of the 6 cells is 273 g. A cell balancing charge management system controlled by the FPGA ensures that the all the individual cells are at a uniform voltage.

A de-rated end-of-life battery capacity of 35.75 Wh is available for use. Of this capacity, 10.73 Wh (30%) is kept as reserve, night-time survival energy usage is estimated at 21 Wh for typical operation in the northern latitudes in the spring season, and approximatley 10 Wh is available for flight. Assuming that 20% of the power is at the peak load of 510 W and 80% is at a continuous load of 360 W, approximately 90 sec of flight is possible. These energy projections represent conservative worst-case end-of-mision battery performance at 0 C initial temperature. More moderate power loads will extend the flight time.

The solar panel is made from Inverted Metamorphic (IMM4J) cells from SolAero Technologies. The cells are optimized for the Mars solar spectrum and occupy a rectangular area with 680 cm^2 of substrate (544 cm^2 active cell area) in a region centered and immediately above the co-axial rotors. This region minimally interferes with the flow through the rotor.

H. Thermal System

The helicopter must survive the cold of the night on Mars where temperatures can drop to -100 C or lower. The most critical component is the battery which is kept above -15 C through the night as it powers Kapton film heaters attached to the battery cells. The avionics boards in the ECM surround the battery and are also kept at an elevated temperature by virtue of their proximity to the warm battery assembly. Insulation around the avionics boards is provided by a carbon-dioxide gap of 3 cm width. Additional insulation can be provided by replacing the carbon-dioxide gas with an Aerogel formulation. The outermost fuselage thermal coating is from Sheldahl with Solar absorptivity $\alpha = 0.8$ and infra-red (IR) emissivity $\epsilon = 0.1$.

In addition to thermal losses through the gas gap (or aerogel), additional losses occur due to conduction in the mast

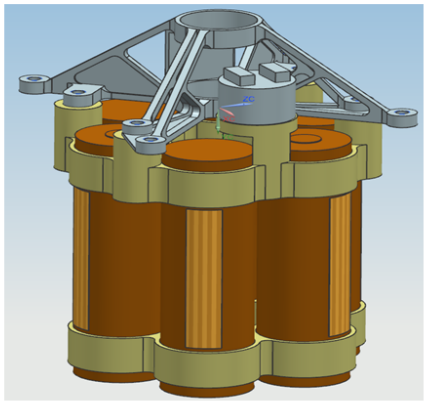

Fig. 12 Battery assembly with Li-Ion cells and bonded thermostat and heaters

as well as through the copper wiring that penetrate the ECM from the mast. To minimize the latter, the wire gauges are selected to be of the thinnest gauges that can still support the current draw during operations without overheating.

Prior to flight, under the control of the FPGA, the thermal system powers on heaters in the motor control boards that have been exposed to the ambient temperatures. The internal battery temperature is brought up to 5 C to allow hi-power energy extraction from the cells. During operation the ECM and battery warm as a result of avionics operations and battery self-heating. However, the thermal inertia of the elements is such that for the short flights of the helicopter, there is no overheating.

V. Concept of Operations

To understand the potential operations of a Mars helicopter technology demonstrator, it is useful to consider as an example, a specific upcoming Mars rover mission and the potential deployment of a helicopter asset as part of that mission. Three landing sites that address the science objectives (seeking habitable conditions and signs for microbial life) of the mission and are safe are being considered for the Mars 2020 Rover mission (as of early 2018). The landing sites (Jezero crater, Northeast Syrtis and the Columbia Hills) are in the equatorial region at relatively low elevation [11, 12]. Extensive characterization by orbital imaging shows the sites to be relatively smooth, flat and with relatively low rock abundance and safe for landing with the sky crane, terrain relative navigation and avoidance system [13]. Several regions of interest (ROI) have been identified at each of the sites that will be targets of extensive surface exploration and the collection and caching of samples for eventual return to Earth. After landing, the rover will begin traversing to the closest ROI. On the way to the ROI, using orbital data, the rover could be directed to areas that likely meet the requirements for deploying the helicopter and flying the technology demonstration sorties. These areas would have to have low slopes and sufficient surface texture for accurate tracking by the demonstrator's navigation filter during flight and few rocks higher than 5 cm to interfere with its landing. The rover would need to image the area being considered at higher resolution than from orbit using stereo rover Navigation camera images to determine if it meets the requirements. If the area for landed helicopter operations is a patch about $10\ m \times 10\ m$ and outbound sorties lengths are 100 m, then analysis of orbital images and stereo digital elevation models indicates that the rover would need to traverse less than 200 m in over 90% of the landing ellipses to find suitable areas for deploying and flying the helicopter.

The technology demonstrator is designed to conduct over a period of 30 sols. After deployment, the fully self-contained helicopter must survive temperature conditions dropping to -100 C at night or lower. It would nominally

undertake daily (depending on solar energy and thermal status) autonomous flights at approximately 11 am local time, with each flight lasting upto 90 sec with flight ranges of upto 300 m at altitudes of approximatley 10 m above the ground. The helicopter is designed to transmit key engineering data as well as high-resolution color images of terrain to a relay station for subsequent re-transmission to Earth. Up-to five technology experiment flights are anticipated during the 30 sol helicopter mission window. Atmospheric conditions expected at the Mars for the nominal flight times have density ranging from 0.014 kg/m^3 to 0.02 kg/m^3, temperatures of approximatley -50 C, and winds up-to a maximum of approximately 10 m/s.

VI. Conclusion

The Mars Helicopter technology demonstrator represents an exciting opportunity to break the aerial dimension in planetary exploration. Successful testing of a prototype under Mars conditions has led to an EDM that is currently undergoing extensive flight-dynamics and environment testing.

Acknowledgments

The research was carried out at the Jet Propulsion Laboratory, California Institute of Technology, under a contract with the National Aeronautics and Space Administration. The authors would like to thank the members of the Mars Helicopter team - MiMi Aung, Chris Bang, Susan Gorton, Joe Melko, Karen Lee, Michael Kokorowski, Jeff Simmonds, Matt Keennon, Ben Pipenberg, Bart Hibbs, Jeremy Tyler, Sara Langberg, Katie Beckwith, Daniel Fugett, Teddy Tzanetos, Fernando Mier-Hicks, Brandon Burns, Greg Carr, Steve Dawson, Christian Liebe, Bill Whitaker, Gorong Gandhi, Jaakko Karras, Patrick Meras, Larry Matthies, Jason Carlton, Saverio D'Agostino, Parviz Danes, Jonathan Denison, Ed Konefat, John Liu, Johnny Lam, Dan Scharf, Guru Singh, Lia Altenbuchner, Tien Nguyen, Steve Yows, Jack Pempejian, Josh Ravich, Taryn Bailey, Michael Pauken, Stefano Cappucci, James Seastrom, Ella Seal, Keith Fields, Brad Kinter, Larry Young, Brian Allan and Berenice Mettler.

References

[1] Grip, H. F., Johnson, W., Malpica, C., Scharf, D. P., Mandić, M., Young, L., Allan, B., Mettler, B., and San Martin, M., "Flight dynamics of a Mars Helicopter," *Proc. European Rotorcraft Forum*, Milan, Italy, 2017.

[2] Lim, C., and Jain, A., "Dshell++: A Component Based, Reusable Space System Simulation Framework," *Proc. Third IEEE International Conference on Space Mission Challenges for Information Technology*, Pasadena, CA, 2009.

[3] Johnson, W., *Rotorcraft Aeromechanics*, Cambridge University Press, 2013.

[4] Johnson, W., "Rotorcraft Aeromechanics Applications of a Comprehensive Analysis," *HeliJapan 1998: AHS International Meeting on Rotorcraft Technology and Disaster Relief.*

[5] Johnson, W., "Rotorcraft Aerodynamic Models for a Comprehensive Analysis," *American Helicopter Society 54th Annual Forum*.

[6] Johnson, W., *Influence of Lift Offset on Rotorcraft Performance*, NASA TP 2009-215404, 2009.

[7] Koning, W. J. F., "Generation of Mars Helicopter Rotor Model for Comprehensive Analyses," *AHS Specialists Conference on Aeromechanics Design for Transformative Vertical Flight*, San Francisco, CA, 2018.

[8] Young, L. A., "Simulated Tiltrotor Aircraft Operation in Close Proximity to a Building in Wind and Ground-Effect Conditions," *Proc. AIAA Paper No. 2015-2700*, 2015.

[9] Grip, H. F., Scharf, D. P., Malpica, C., Johnson, W., Mandić, M., Singh, G., and Young, L., "Guidance and Control for a Mars Helicopter," *Proc. AIAA Guidance, Navigation, and Control Conference*, Kissimmee, FL, 2017.

[10] Canham, T., *Instrument Software Framework*, JPL, 2015.

[11] Golombek, M. P., Grant, J. A., Farley, K. A., and Chen, A., "Science objectives, engineering constraints, and landing sites proposed for the Mars 2020 rover mission (expanded abstract)," *46th Lunar and Planetary Science, Abstract 1653*, Lunar and Planetary Institute, Houston, 2015.

[12] Golombek, M. P., Grant, J. A., K. A. Farley, K. W., Chen, A., Otero, R. E., and Ashley, J. W., "Downselection of landing sites proposed for the Mars 2020 Rover Mission (expanded abstract)," *47th Lunar and Planetary Science, Abstract 2324*, Lunar and Planetary Institute, Houston, 2016.

[13] Golombek, M. P., Otero, R. E., Heverly, M. C., Ono, M., Williford, K. H., Rothrock, B., Milkovich, S., Almeida, E., Calef, F., Ashley, J., and Chen, A., "Characterization of Mars Rover 2020 prospective landing sites leading up to the second downselection: (expanded abstract)," *48th Lunar and Planetary Science, Abstract 2333*, Lunar and Planetary Institute, Houston, 2017.